# On the effect of blade deformations on the aerodynamic performance of wind turbine rotors subjected to yawed inflow

IOP Conf. Series: Journal of Physics: Conf. Series **1037** (2018) 022030 doi:10.1088/1742-6596/1037/2/022030

# On the effect of blade deformations on the aerodynamic performance of wind turbine rotors subjected to yawed inflow

**B. Dose[1,2], H. Rahimi[1,2], B. Stoevesandt[2], J. Peinke[1,2], J.G. Schepers[3]**

[1] ForWind, Institute of Physics, University of Oldenburg, Germany
[2] Fraunhofer IWES, Oldenburg, Germany
[3] Energy research Centre of the Netherlands, Petten, Netherlands

E-mail: bastian.dose@uni-oldenburg.de

**Abstract.**

This work is aimed to investigate the effects of elastic blade deformations on the aerodynamics of large wind turbine rotors subjected to yawed inflow. Due to the increasing rotor size and advanced light weight blade designs, significant blade deflections can be observed on a regular basis for modern wind turbines. However, especially for complex flow situations like yawed inflow, the role of blade deformations is still not completely understood. In this paper, numerical simulations are conducted on the DTU 10 MW reference wind turbine to gain a better understanding of the involved phenomena. Results are obtained by two numerical methods of different fidelity. First, by the aero-elastic simulation tool FAST, which is based on the low fidelity Blade Element Momentum Theory (BEM) and makes use of common skewed wake correction models. Secondly, by a high-fidelity framework which couples the open-source Computational Fluid Dynamics (CFD) toolbox OpenFOAM with the in-house geometrically non-linear beam solver BeamFOAM. The evaluation of the results is based on the analysis of azimuthal variations of the sectional forces along the blade span and reveals a generally good agreement between the used numerical approach in terms of force amplitudes and variation phases. However, especially for cases of larger yaw angles, the BEM models clearly over-predict the variation amplitudes of the forces up to 40% in the outer blade part.

## 1. Introduction

Over the last years, a clear trend towards larger rotor diameters can be observed. The next generation of wind turbines will make use of slender and highly flexible rotor blades, which are based on advanced light weight designs [1]. To make these machines a success, the accurate aerodynamic and aero-elastic modeling during the design phase can be considered as crucial. At the same time, the Blade Element Momentum (BEM) theory is expected to remain the industrial method of choice for the next years. Being a two-dimensional and steady theory, BEM based load calculations require the use of numerous correction models to overcome the limits of the underlying simple theory. However, due the empirical nature of most engineering models, which are often based on findings obtained by rather small experimental wind turbines, their validity for the modeling of large rotors is currently under discussion [1, 2, 3]. Consequently, Computational Fluid Dynamics (CFD) are increasingly used to re-investigate the modeled phenomena for large rotor scales. An example is the work of Rahimi et al. [4], which showed that the high fidelity of

CFD simulations can help to improve the performance of engineering models at the inner blade region for large rotor sizes. However, the structural deformations are usually not considered in the frame of the mentioned investigations and recent CFD based aero-elastic studies showed that structural deformations can play a major role for the azimuthal variation of loads [5, 6, 7, 8, 9]. In this work, the validity of state-of-the-art skewed wake correction models in combination with structural deformations will be investigated. Hereby two numerical methods of different fidelity, namely BEM and CFD, are used to simulate a large wind turbine subjected to yawed inflow at different angles. Both rigid and aero-elastic computations are performed to investigate the effect of large blade deflections on the aerodynamic rotor performance.

## 2. Investigated wind turbine model

In this work, the DTU 10 MW reference wind turbine with a rotor diameter of 178.3m is used for the performed numerical studies [10]. The three bladed horizontal axis wind turbine was investigated within large European research projects like Avatar [11] or Innwind [12] and can be considered as one of the current state-of-the-art wind turbine designs, which are available within the wind energy research community. Furthermore, due to its large blade lengths of 78m, relevant structural deformations can be expected. Within this paper, only the wind turbine rotor is modeled, the tower and nacelle geometries are not considered. Furthermore, the prescribed shaft tilt is not taken into account. Since the focus of this paper is on the effect of structural blade deformations, the presence of gurney flaps in the inner blade part is neglected in all used numerical models. In total, two rotor configurations are simulated. First, the rigid rotor with three straight blades and without blade cone is investigated and serves as a reference. In a second step, the flexibility of the blades is taken into account. For all aero-elastic simulations, both pre-bending and blade cone, as described in the DTU reference [10], are considered. Figure 1 illustrates the rotor geometries simulated by means of CFD, the straight blade geometry is shown in light gray. All presented simulations in this work are performed for a laminar inflow wind speed of 11 m/s and a rotational speed of 8.837 rpm. Three different yaw misalignment angles, namely 15°, 30° and 45° are investigated. Further relevant data is listed in Table 1.

(a) Isometric view. (b) Side view.

Figure 1: Simulated rotor geometry. The straight blade geometry, used for the rigid CFD simulations, is shown in light gray.

Table 1: Overview DTU 10 MW reference turbine [10].

| Parameter | Value |
|---|---|
| Number of blades | 3 |
| Rotor diameter | 178.3 m |
| Simulated wind speed | 11 m/s |
| Simulated rotational speed | 8.837 rpm |
| Blade pitch angle | 0° |
| Blade cone angle | 2.5° |
| Shaft tilt angle | 0° |
| Blade length (straight) | 86.37 m |
| Blade mass | 41716 kg |

## 3. Computational Setup

*3.1. Used numerical approaches*

*3.1.1. BEM:* As a reference, representing a standard approach used in industrial rotor design, the BEM-based code FAST v8 is used [13]. The modeling of the aerodynamic loads in FAST is achieved by the AeroDyn module in version 14 [14], the structural response is computed by the structural solver ElastoDyn. It should be noted, that ElastoDyn does not consider torsional deformations, which are expected to reach significant amounts for the investigated wind turbine [12]. Furthermore, the aerodynamic induction is calculated based on the undeformed blade geometry. Two different approaches are utilized to model the skewed wake effect within the FAST simulations. First, the skewed wake correction of Glauert, which is based on his work on the autogyro flight vehicle, is used [15]. He proposed the following relation in order to correct the induction at the blades for non-axial conditions:

$$a = a_{average}\left(1 + K\frac{r}{R}sin\phi\right), \tag{1}$$

where $K$ is a function of the skew wake angle of the wind turbine and $\phi$ denotes the azimuthal angle. This model is developed based on the assumption, that the variation in induced velocity is purely sinusoidal and caused by the skewed tip vortices. Many attempts were made in the past to improve the $K$-factor in the original model by more accurate modeling of the wake expansion and deflection. In this work, the modification of Pitt and Peters (PP) is used [14]. Figure 2 illustrates the used convention for the azimuthal angle $\phi$ in this work.

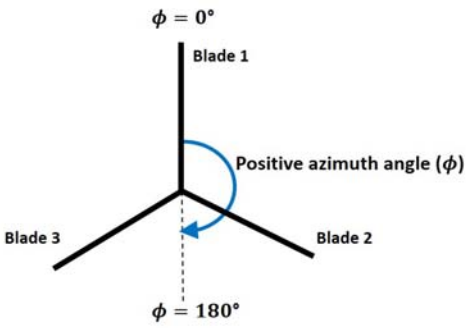


Figure 2: Convention for the azimuthal angle $\phi$ in this work.

As a second approach, the Generalized Dynamic Wake (GDW) model is utilized, which originates from helicopter aerodynamics and is based on a potential flow solution for the Laplace's equation [14]. The main advantage of the method is a more general distribution of pressure across the rotor plane than obtained by BEM models. It physically includes the modeling of the dynamic wake effect, tip losses and the skewed wake effect [14].

*3.1.2. CFD:* To model the aerodynamics of wind turbine subjected to yawed inflow on a higher fidelity level, a fluid-structured coupled CFD solver is utilized [9, 16]. Coupling the open source CFD code OpenFOAM [17] with the in-house structural beam solver BeamFOAM, which is based on the Geometrically Exact Beam Theory (GEBT) [18, 19]. The method allows the simulation of complex flow situations without the need of empirical correction models, which can introduce additional uncertainties. The performance of the fluid-structure coupling framework was investigated in Ref. [16, 9]. The solution for the flow field is achieved based on solving the incompressible Unsteady Reynolds-Averaged Navier-Stokes (URANS) equations. The closure problem is treated by the use of the k-$\omega$-SST turbulence model by Menter [20]. The flow is assumed to be fully turbulent, therefore the laminar-turbulent transition in the boundary layer is not considered. The coupling of velocity and pressure is performed using the merged SIMPLE-PISO algorithm PIMPLE, which is available in the OpenFOAM package. The convective terms are discretized using a second-order accurate linear-upwind scheme and the discretization in time is performed using a second-order backward formulation. The fluid-structure coupling is performed once per time step. All conducted CFD simulations are time-accurate and more than 20 full rotor revolutions are simulated for each case to reach converged wake states. The simulations are performed in parallel on 240 Intel Xeon CPU E5-2650 cores (10 nodes) with a clock frequency of 2.2 Ghz at the EDDY cluster at the University of Oldenburg. Utilizing a azimuthal step size of 0.7°, three revolutions per 24h were achieved for both the rigid and fluid-structure coupled computations.

*3.2. CFD grid*

The fluid domain is discretized using an unstructured grid, consisting mostly of hexahedral cells. To achieve the complete grid, three blade meshes, a rotor mesh and a farfield mesh are connected using Arbitrary Mesh Interfaces (AMI) [17]. In the first step, the blade meshes are created using the inhouse tool BladeBlockMesher (BBM) [21], which combines sectional 2D-meshes to a complete 3D blade mesh and creates fully structured meshes utilizing hexahedrons only. The utilized blade mesh is generated with a spanwise resolution of 300 cells, a chordwise resolution of 260 cells and 40 cells normal to the blade surface. In order to limit the cell aspect ration in radial direction, adaptive wall functions are being applied. The rotor and farfield meshes are generated and combined using the inhouse meshing tool windTurbineMesher, which uses a provided blade mesh from BBM or other meshing tools like Pointwise [22] to create the meshes of complete wind turbines including hub, nacelle and tower geometries. Since the windTurbineMesher utilizes the meshing tool snappyHexMesh [17], included within the OpenFOAM framework, the rotor and farfield meshes are of unstructured nature, consisting mainly of hexahedras and split-hexahedras. To reduce the amount of cells required to resolve the wind turbine wake, the windTurbineMesher utilizes pre-defined ring-shaped mesh refinements in the region of the tip and root vortices instead of uniform wake refinements. Table 2 provides an overview about the numerical domain dimensions and used cell numbers for the rigid CFD simulations. The meshes used for the aero-elastic runs are based on identical refinement levels and contain a comparable amount of cells. The final grid refinement levels are selected based on a performed grid dependency study, which is not presented here. Figure 3 illustrates the general shape and dimensions of the utilized CFD domain and a visualization of the used grid refinement strategy.

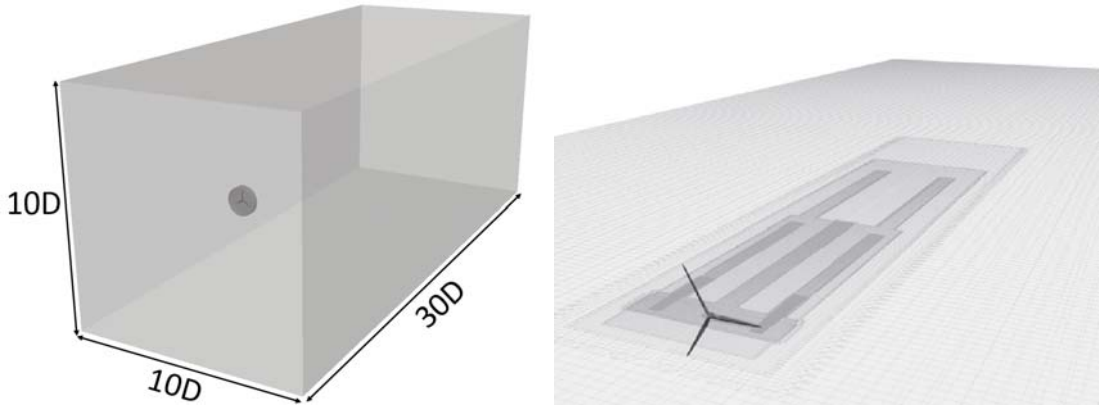


(a) Shape and dimensions of numerical domain. (b) Nested mesh refinement strategy.

Figure 3: Computational domain for the performed CFD simulations.

Table 2: Mesh details for the rigid investigated cases. The listed numbers are given in units of million cells.

| Blade meshes | Rotor mesh | Farfield mesh | Total cells |
|---|---|---|---|
| 3 x 3.5 | 8.0 | 23.0 | 41.5 |

*3.3. Structural setup*

The blade structure is modeled based on the structural beam section properties provided in the reference report and all 51 provided structural beam section properties are taken into account. The modeling in BeamFOAM is based on iso-parametric three-node GEBT beam elements utilizing quadratic element shape functions. To improve the comparability of the obtained results, off-diagonal entries of the 6x6 cross sectional stiffness matrix are neglected. As a consequence, the blades behave torsionally stiffer and due to the rather small torsional deformations, the obtained results can then be better compared to the ElastoDyn computation. In Table 3, the calculated natural frequencies of the isolated blade are listed and compared to reference values. The structural damping ratio is specified according to the reference report with a logarithmic decrement of 3%. The calculated integrated mass of each wind turbine blade within BeamFOAM accounts to 41722 kg, which is in a good agreement with the reference listed in Table 1. Gravitational loading acting on the structure is included within all fluid-structure coupled simulations. The following convention will be used for the rest of this work: A positive flapwise deflection is pointing downstream, while a positive edgewise deflection points in the direction of the leading edge.

## 4. Results

The first part of the result evaluation deals with the comparison of the blade deflections, which are predicted by the three different numerical models. The main focus is on the prediction of the azimuthal variation of the aerodynamic forces and the structural deflections. As such, the difference in the mean values of the above mentioned quantities is less relevant for this work and all presented results are normalized by their mean values, which are obtained by averaging over one revolution. Moreover, since a complete presentation of all the results for all sections cannot be provided within the scope of this paper, only the selected cases endeavor to represent the

Table 3: Calculated natural frequencies of the isolated DTU 10 MW reference turbine blade [23].

| Mode | Reference [Hz] | BeamFOAM [Hz] |
|---|---|---|
| 1st Flap | 0.615 | 0.614 |
| 1st Edge | 0.971 | 0.937 |
| 2nd Flap | 1.764 | 1.744 |
| 2nd Edge | 2.857 | 2.795 |
| 1st Torsion | 5.753 | 5.714 |

results for all sections across all yaw angles. For the presented yawed angles, the upwind side of the rotor plane is between 180° to 360°, and the downwind side is between 0° to 180°. At 0° azimuth, the blade is point upwards (12 o'clock), the direction of rotation is clockwise. Figure 4 illustrates the variation of the flapwise and edgewise blade deflections over one rotation, sampled at the blade tip. Both BEM approaches are listed here as one entry, since the deviations between the two in terms of tip deflections are very small. Compared to the fluid-structure coupled CFD solver, it can be noticed that the phases of variations for both edgewise and flapwise blade deflections are in a good agreement. However, the amplitude of the variations are predicted larger by the BEM models. These deviations are believed to be caused mainly by two reasons. First, as it is shown in the next part of result section, the BEM methods generally over-predict the variation amplitude of the aerodynamic forces, which results in larger deflection amplitudes. Secondly, the ElastoDyn module is based on a linear structural solver, while the fluid-structure coupled CFD framework is based on BeamFOAM, which is of non-linear nature. It can be observed that all approaches predict the minimum blade deflections on the downwind side of the rotor (0-180° azimuth) and the maximum blade deflections on the upwind side (180-360° azimuth). Furthermore, the variation amplitudes significantly increase with larger yaw angles.

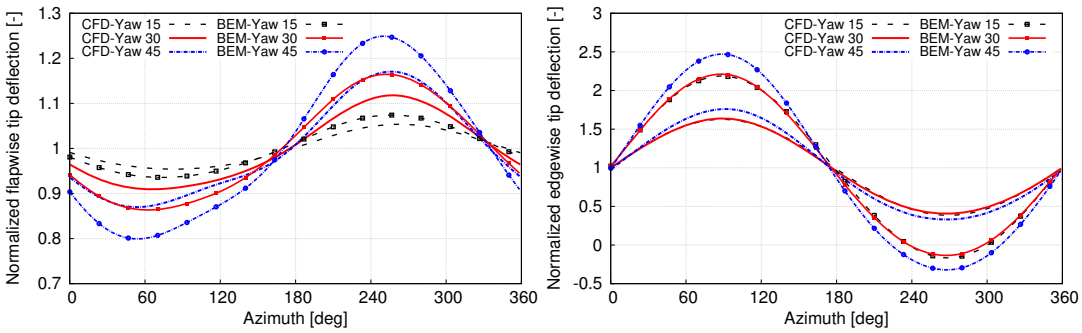


(a) Normalized flapwise tip deflection. (b) Normalized edgewise tip deflection.

Figure 4: Normalized flapwise and edgewise tip deflections over one revolution. The normalization of the quantities is performed based on their respective mean values, which are averaged over one rotor revolution.

In the following, the rotor performance is evaluated based on three different yaw angles.

- Yaw angle 15°: Figure 5 illustrates the distribution of the normal and tangential forces over azimuth for mid span (60% radius) and the outer blade part (90% radius) for a yaw angle of 15°. At 60% span, both CFD runs and both BEM computations under use of the GDW

model predict the variation of the normal force in a very similar matter. The forces fluctuate approximately 5% around their mean values and structural blade deformations lead in for both approaches to a slight phase shift of the variations towards the upwind side. However, the amplitude of the fluctuations seems not to be affected by the aero-elasticity. In contrast to that, the model by Pitt and Peters shows larger deviations. While the phase is computed similar, the amplitude of the fluctuations are predicted twice as large. The reason for this behavior is the influence of the root vortex, which is not taken into consideration by the model, but still has an effect at mid span [4]. In contrast to that, both CFD and the GDW are able to capture this phenomena and deviate from pure sinusoidal shape of the Pitt and Peters model. A similar trend can be observed for the tangential forces at mid span. The results obtained by CFD and GDW are again very similar and the PP model is deviating from both others. It should be further noted, that the amplitude of the fluctuations of the tangential forces is predicted almost twice as large as the normal forces. Furthermore, besides a slight phase shift, the structural deformations result in an increase of the amplitude of the variation if the tangential forces of around 5% for both BEM approaches and the CFD. At 90% span, similar findings can be revealed. Since the influence of the tip vortex is

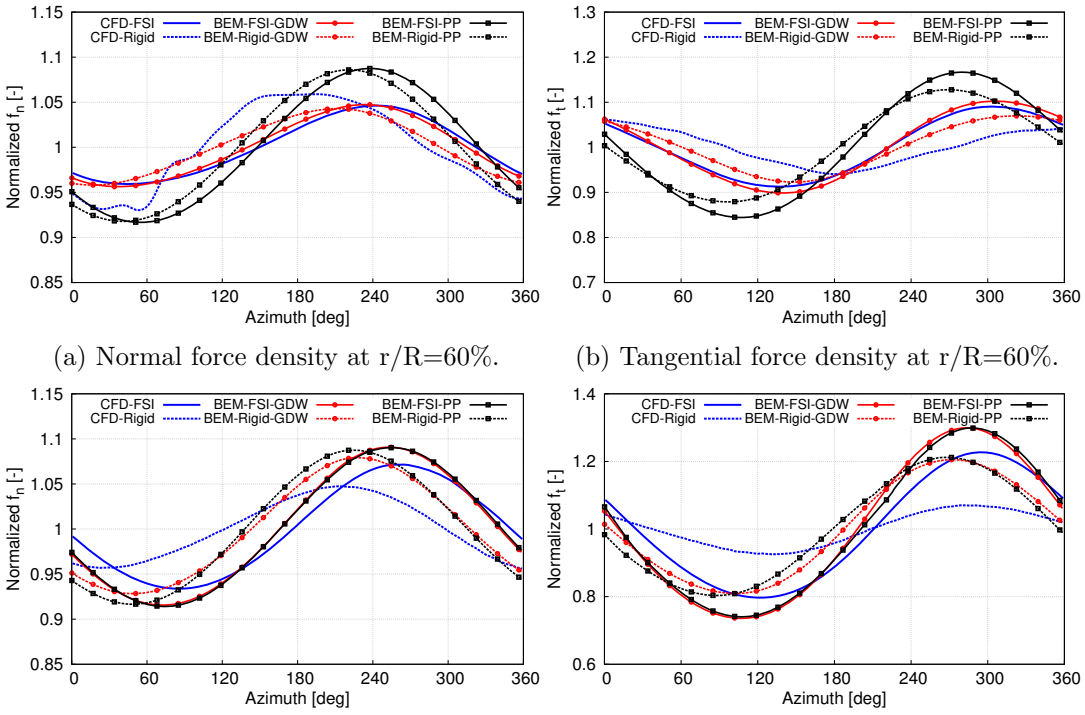


(a) Normal force density at r/R=60%.

(b) Tangential force density at r/R=60%.

(c) Normal force density at r/R=90%.

(d) Tangential force density at r/R=90%.

Figure 5: Normalized forces densities in normal and tangential directions for a yaw angle of 15°.

dominant near the blade tip, the model of PP shows an almost identical behavior compared to the GDW for both forces. However, compared to the reference CFD results, they overpredict the force variations. As before, the consideration of structural deformations results in a phase shift of around 30° towards the upwind side and in a clearly increased amplitude of the tangential forces. The main reason for this phenomena is believed to be the relative motion of the blades caused by the variation of the deflections in edgewise and flapwise directions. This motion influences the aerodynamic forcing, which can lead to slight shifts of the variation phase. It can further be observed, that the consideration of aero-elastic

effects has a more significant effect in the CFD based results, although the blade motions are predicted stronger in the BEM based approaches (see Figure 4).

- Yaw angle 30°: Figure 6 shows the distribution of the normal and tangential forces over azimuth for a yaw angle of 30°. Although all methods still predict a similar trend, deviations between the methods and the influence of the aero-elasticity are now more pronounced. At 60% span, CFD and BEM-GDW predict in general again a similar phase and amplitude of the force variations. As before, PP clearly over-predicts amplitude of both forces compared to the other methods. However, it can be observed that the consideration of the aero-elastic blade response results in larger differences compared to the previous case of 15° yaw. In terms of normal forces, again a small phase shift but also a slight increase in force amplitude is predicted for the CFD-FSI based results. Both phenomena are also captured by the GDW model in the same manner. For the tangential forces, the implications of the blade deformations are much larger. In terms of amplitude, the CFD-FSI predicts an increase of approximately 10% on the upwind side, while the downwind side seems less effected. The increase in amplitude is also captured by the GDW code, however the phase of the variations start to deviate. Especially for the rigid computations, CFD and GDW show a clear shift in phase. Interestingly, the aero-elastic computations agree well in terms of phase and both approaches predict a slight phase shift of the signal towards the downwind side. The model by PP is again strongly over-predicting the amplitude, furthermore the consideration of the aero-elastic response leads to a phase shift to the upwind side.

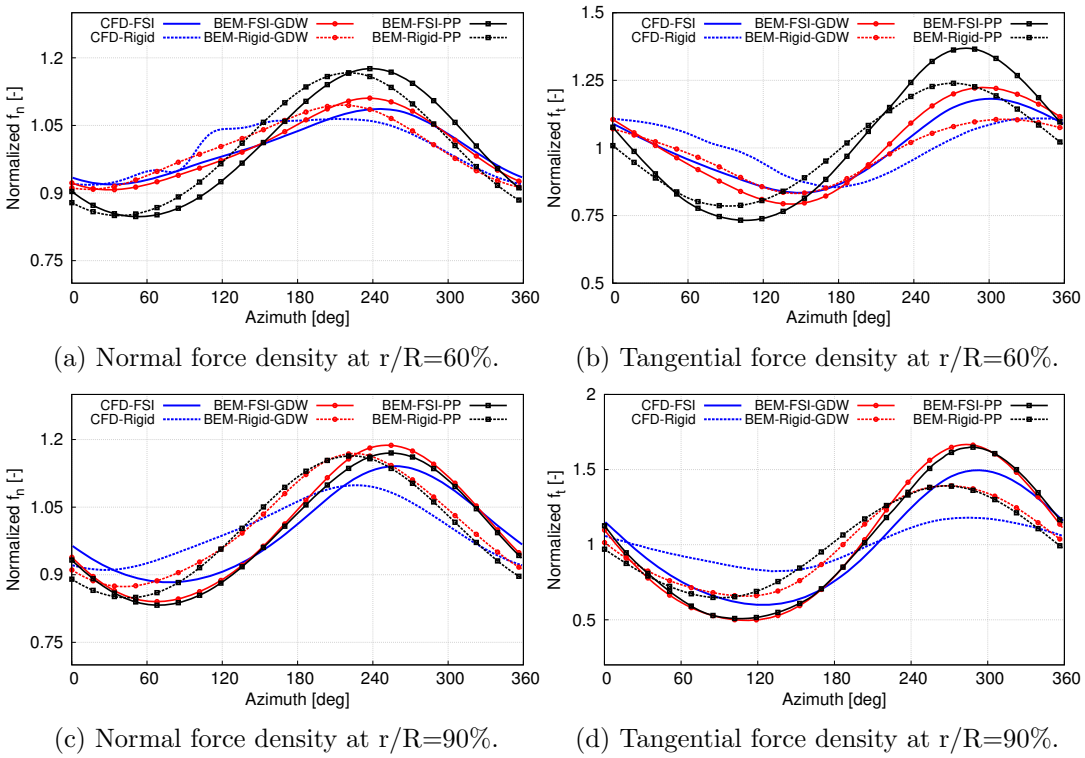


(a) Normal force density at r/R=60%.

(b) Tangential force density at r/R=60%.

(c) Normal force density at r/R=90%.

(d) Tangential force density at r/R=90%.

Figure 6: Normalized forces densities in normal and tangential directions for a yaw angle of 30°.

At 90% span, the general picture is similar to the yaw angle of 15%. All BEM based approaches agree well with each other but clearly over-predict the variation amplitude compared to the CFD solvers. This is especially the case for the tangential forces, which

again shows much more pronounced fluctuations than the normal forces. However, the phase is predicted generally well. In addition it can be observed that the effect of the structural deformations increases the variation amplitudes by 10% - 30%. As in the case of 15° yaw, the CFD-based approach predicts a more significant effect of the structural dynamics compared to the BEM simulations.

- Yaw angle 45°: For the case of 45 degrees yaw, the previously found trends are observed to a larger extent (see Figure 7). Since for those large yaw angles, the BEM simulations operate increasingly out of their valid range, their results are now clearly deviating from the reference CFD results. At 60% span, both BEM based approaches over-predict the amplitude of both normal and tangential forces. In the case of tangential forces, deviations up to 30% can be observed in the case of the PP model. However, also the GDW model shows now larger differences compared to the CFD approaches. In addition it can be observed that also the structural deformations start to play a more dominant role, leading to larger differences between the rigid and aero-elastic computations. At 90% span, large force variations are predicted by all codes. The consideration of the aero-elastic blade response increases the force fluctuations by 50% to 60%, which can be explained by the large relative blade velocities caused by large flapwise and edgewise deflections (see Figure 4). However, as found also for the previously described yaw cases, both the phase of the force variations and the effect of the structural deformations are generally well captured by the computationally efficient BEM simulations.

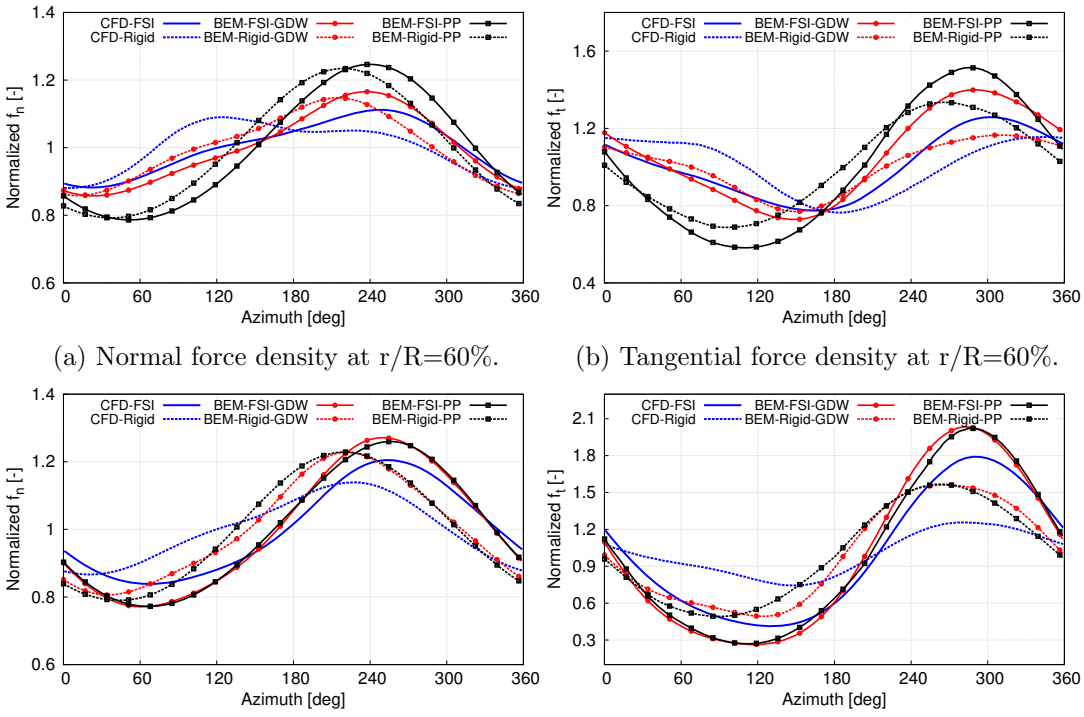


(a) Normal force density at r/R=60%.

(b) Tangential force density at r/R=60%.

(c) Normal force density at r/R=90%.

(d) Tangential force density at r/R=90%.

Figure 7: Normalized forces densities in normal and tangential directions for a yaw angle of 45°.

## 5. Conclusion

In this work, the performance of the DTU 10 MW reference wind turbine rotor has been evaluated for different yaw misalignment angles. The numerical simulations were performed

using methods of different fidelity and all methods were used in a rigid and aero-elastic modes to investigate the influence of structural blade deflections on the aerodynamic rotor performance. The following conclusions could be drawn from the result analysis and discussion:

- At mid span, the BEM GDW method generally agrees well with CFD for both the rigid and aero-elastic runs in terms of force variations and phase. However, the model of Pitt and Peters clearly over-predicts the variation amplitudes, which might be caused by the neglect of the root vortex. The impact of the structural deformations is much more pronounced for the tangential forces and leads in all cases to an increase of 5% - 10% of the force variation amplitudes. Furthermore, the influence of the structural deformations gets more dominant with increasing yaw angle.
- In the outer blade part, both BEM models predict very similar force variation amplitudes and phases. This can be explained by the dominant influence of the tip vortex, which is considered by both skew wake models. However, for all investigated cases, the BEM calculations clearly over-predict the variation amplitudes of the forces, which should be addressed in the future. With increasing yaw angles, the consideration of the aero-elastic effects results in clearly increased forces variations. Especially for the tangential forces, differences up to 30%-40% could be shown. In general, both BEM approaches capture the effect of blade deflections on the aerodynamic loading in a similar manner to CFD, although the latter predicts a stronger influence. Therefore it is believed, that the relative motion of the blade due to the deformations is more dominant than changes caused by the changing tip vortex trajectory, which is only captured by the CFD approaches.
- In the next step, the effect of torsional deformations should be investigated in more detail. However, it is believed that the effect of torsional blade deformations should be captured by the BEM based approaches.

## Acknowledgments

The simulations were performed at the HPC Cluster EDDY, located at the University of Oldenburg (Germany) and funded by the Federal Ministry for Economic Affairs and Energy (Bundesministeriums fuer Wirtschaft und Energie) under grant number 0324005.

## References

[1] Schepers J G 2016 *Journal of Physics: Conference Series* vol 753 (IOP Publishing) p 022017 ISSN 17426596
[2] Schepers J G 2012 *Engineering models in wind energy aerodynamics: Development, implementation and analysis using dedicated aerodynamic measurements* Doctoral thesis TU Delft URL http://repository.tudelft.nl/assets/uuid:92123c07-cc12-4945-973f-103bd744ec87/PhD_Schepers.pdf
[3] Rahimi H, Hartvelt M, Peinke J and Schepers J G 2016 *Journal of Physics: Conference Series* vol 753 (IOP Publishing) p 22016
[4] Rahimi H, Garcia A M, Stoevesandt B and Schepers J G 2018 *Wind Energy*
[5] Yu D O and Kwon O J 2014 *Journal of Physics: Conference Series* **524** 012046 ISSN 1742-6596 URL http://stacks.iop.org/1742-6596/524/i=1/a=012046?key=crossref.bf4f8092d8c9fc43a624cdea7e74eb5a
[6] Heinz J C, Sørensen N N, Zahle F and Skrzypiński W 2016 *Wind Energy* **19** 2041–2051 ISSN 10991824 (*Preprint* arXiv:1006.4405v1)
[7] Heinz J C, Sørensen N N and Zahle F 2016 *Wind Energy* **19** 2205–2221 ISSN 10991824 (*Preprint* arXiv:1006.4405v1) URL http://onlinelibrary.wiley.com/doi/10.1002/we.1608/full http://doi.wiley.com/10.1002/we.1976
[8] Sayed M, Lutz T, Krämer E, Shayegan S, Ghantasala A, Wüchner R and Bletzinger K U 2016 *Journal of Physics: Conference Series* **753** 042009 ISSN 1742-6588 URL http://stacks.iop.org/1742-6596/753/i=4/a=042009?key=crossref.91ebfaccb4f833531dbfb4e9fea33e84
[9] Dose B, Rahimi H, Herráez I, Stoevesandt B and Peinke J 2018 *Submitted to Renewable Energy*
[10] Bak C, Zahle F, Bitsche R, Kim T, Yde A, Henriksen L C, Natarajan A and Hansen M H 2013 Description of the DTU 10 MW Reference Wind Turbine Tech. Rep. July Technical University of Denmark Wind Energy Roskilde, Denmark (*Preprint* arXiv:1011.1669v3) URL https://dtu-10mw-rwt.vindenergi.dtu.dk

[11] 2016 AVATAR: Advanced Aerodynamic Tools for Large Rotors URL http://www.eera-avatar.eu/
[12] 2016 INNWIND.EU: Design of state of the art 10-20MW offshore wind turbines URL http://www.innwind.eu/
[13] Jonkman J M and Buhl Jr M L 2005 *National Renewable Energy Laboratory, Golden, CO, Technical Report No. NREL/EL-500-38230*
[14] Moriarty P J and Hansen a C 2005 *Renewable Energy* **15** 500–36313 ISSN 00664189 URL http://www.nrel.gov/docs/fy05osti/36881.pdf
[15] Glauert H, Committee A R and Others 1926 *A general theory of the autogyro* vol 1111 (HM Stationery Office)
[16] Dose B, Rahimi H, Herráez I, Stoevesandt B and Peinke J 2016 *Journal of Physics: Conference Series* **753** 022034 ISSN 1742-6588 URL http://stacks.iop.org/1742-6596/753/i=2/a=022034?key=crossref.fc74bea82ffb394aa57e1b4d3c9bf4ad
[17] The OpenFOAM Foundation Ltd 2016 OpenFOAM: The Open Source Computational Fluid Dynamics (CFD) Toolbox v4.1.0 URL https://openfoam.org/
[18] Simo J C 1985 *Computer Methods in Applied Mechanics and Engineering* **49** 55–70 ISSN 00457825
[19] Bauchau O A 2010 *Flexible Multibody Dynamics* vol 176 ISBN 940070335X URL http://books.google.com/books?id=Pn94Czlg7VUC&pgis=1
[20] Menter F R, Kuntz M and Langtry R 2003 *Turbulence Heat and Mass Transfer 4* **4** 625–632 ISSN 1662-8985 URL http://cfd.mace.manchester.ac.uk/flomania/pds_papers/file_pds-1068134610Menter-SST-paper.pdf
[21] Rahimi H, Daniele E, Stoevesandt B and Peinke J 2016 *Wind Engineering* **40** 148–172 ISSN 0309-524X
[22] 2017 Pointwise - User manual Tech. rep. Pointwise, Inc URL www.pointwise.com
[23] Pavese C, Wang Q, Kim T, Jonkman J M and Sprague M A 2015 *Proceedings of the EWEA Annual Event and Exhibition 2015* (European Wind Energy Association (EWEA)) p 9